SIMULATING VENTED HYDROGEN DEFLAGRATIONS: IMPROVED MODELLING IN THE CFD TOOL FLACS-HYDROGEN

Lucas, M.[1], Atanga, G.[1], Hisken, H.[1] and Skjold, T.[2]
[1] Gexcon, Fantoftvegen 38, 5072 Bergen, Norway, melodia@gexcon.com
[2] University of Bergen, Allégaten 55, 5007 Bergen

ABSTRACT

This paper describes validation of the computational fluid dynamics tool FLACS-Hydrogen. The validation study includes data from the vented deflagration experiments performed in 20-foot shipping containers as part of the project *Improving hydrogen safety for energy applications through pre-normative research on vented deflagrations* (HySEA), funded by the Fuel Cells and Hydrogen Joint Undertaking (FCH 2 JU). The paper presents results for tests involving inhomogeneous hydrogen-air clouds generated from realistic releases. Using FLACS-Hydrogen with the new numerical solver Flacs3 resulted in significantly improved predictions of the peak overpressures, compared to results obtained with the standard Flacs2 solver. For both experiments and simulations, the peak overpressures for stratified mixtures were higher than for homogeneous mixtures with the same amount of hydrogen.

1.0 INTRODUCTION

Fires and explosions represent a significant hazard for hydrogen energy applications, and specific measures are often required for reducing the risk to a tolerable level. Explosion venting is a frequently used measure for mitigating the consequences of hydrogen deflagrations in confined systems. Whereas most enclosures used for hydrogen applications in industry are inherently congested, most of the experiments that have been used for validating the engineering models in international standards, such as EN 14994 [1] and NFPA 68 [2], were performed with empty vessels. Internal congestion can significantly influence the chain of events in vented hydrogen deflagrations. The effect of congestion on flame acceleration due to enhanced turbulence generation and flame surface area increase due to geometry-induced flame instabilities can be challenging to represent in empirical correlations.

In principle, computational fluid dynamics (CFD) simulations can account for the effect of obstacles and the presence of vent panels on the flame acceleration and overpressure generated in vented deflagrations. However, for risk assessments in industry, it is necessary to estimate the consequences of numerous large-scale scenarios within a limited time frame. For such applications, it is not possible to resolve all relevant spatial and temporal scales of the geometry and the physical phenomena involved. To obtain sufficiently accurate predictions, while retaining acceptable simulation times, several commercial simulation tools rely on the so-called porosity/distributed resistance (PDR) concept. Within the PDR framework, sub-grid geometry is represented as area and volume porosities (denoting the degree of "openness" for each grid cell). This paper summarises the results from an extensive validation study that was undertaken for the newly developed numerical solver Flacs3, which includes updated sub-grid models for premixed combustion [3]. The empirical data include the vented deflagration experiments performed in 20-foot shipping containers as part of the HySEA project, funded by the Fuel Cells and Hydrogen 2 Joint Undertaking. The discussion highlights the predictive capabilities and inherent limitations of the model system and outlines the strategy for further work.

2.0 FLACS-HYDROGEN

FLACS-Hydrogen is a subversion of the CFD tool FLACS [3] for hydrogen safety applications that was first developed in connection with the Network of Excellence (NoE) HySafe, funded by the European Commission. The model has later been improved and validated for hydrogen applications.

This paper compares two versions of FLACS-Hydrogen: FLACS *v10.9* and FLACS *v11 beta*. The Flacs2 solver, which is used in the commercial release FLACS *v10.9*, is replaced by the Flacs3 solver in the FLACS *v11 beta* version. Both the Flacs2 and Flacs3 are PDR solvers that apply the SIMPLE numerical technique to handle the pressure-velocity coupling. The governing equations are discretized on a structured Cartesian mesh [4] [5]. In Flacs2, the pre-processor *Porcalc* computes the area and volume porosities. In Flacs3, the FLACS Geometry Calculator (FGC) has replaced *Porcalc*. In addition to porosities, FGC calculates the geometrical length scale (*GLS*) used by the combustion model. A first-order backward Euler scheme controlled by Courant–Friedrichs–Lewy (CFL) numbers is used for time-stepping in both solvers.

Both Flacs2 and Flacs3 include additional terms for estimating turbulence generation by flow past sub-grid objects, a combustion model based on the flamelet approach, and a numerical flame model that applies an artificially thickened flame front [6]. The next paragraphs outline the main differences in the modelling approaches between Flacs2 (FLACS *v10.9)* and Flacs3 (FLACS *v11 beta)*.

Turbulence modelling

The default turbulence model for dispersion and explosion in both solvers is the standard *k-ε* model [7]:

$$\frac{\partial}{\partial t}(\beta_v \rho k) + \frac{\partial}{\partial x_i}(\beta_j \rho u_i k) = \beta_v P_k - \beta_v \rho \varepsilon + \frac{\partial}{\partial x_i}\left[\beta_j \frac{\mu_{eff}}{\sigma_k}\frac{\partial k}{\partial x_i}\right] \text{ and} \quad (1)$$

$$\frac{\partial}{\partial t}(\beta_v \rho \varepsilon) + \frac{\partial}{\partial x_i}(\beta_j \rho u_i \varepsilon) = \beta_v P_\varepsilon - \beta_v C_{2\varepsilon} \rho \frac{\varepsilon^2}{k} + \frac{\partial}{\partial x_i}\left[\beta_j \frac{\mu_{eff}}{\sigma_\varepsilon}\frac{\partial \varepsilon}{\partial x_i}\right], \quad (2)$$

where β_v and β_j are the volume and the surface area porosities, respectively, ρ is the density, k is the turbulence kinetic energy, u_i is the velocity in the i^{th} direction, P_k is the production of turbulence kinetic energy, ε is the dissipation rate of turbulence kinetic energy, μ_{eff} is the effective dynamic viscosity, P_ε is the production of dissipation rate of turbulence kinetic energy, and $C_{2\varepsilon}$, σ_k and σ_ε are model constants.

Combustion modelling

The model for premixed combustion in both Flacs2 and Flacs3 consists of

- a numerical flame model,
- a burning velocity correlation model,
- a combustion length-scale model, and
- a flame wrinkling model.

These components will be briefly described below, highlighting differences and similarities between the two solvers.

The numerical flame model

In the present work, the same numerical flame model is used in both Flacs2 and Flacs3. The conservation equation for the fuel mass fraction Y_F is expressed as:

$$\frac{\partial}{\partial t}(\beta_v \rho Y_F) + \frac{\partial}{\partial x_j}(\beta_j \rho u_j Y_F) = \frac{\partial}{\partial x_j}\left(\beta_j \rho D \frac{\partial Y_F}{\partial x_j}\right) + R_F. \quad (7)$$

Here the diffusion coefficient, D, and the chemical reaction source term, R_F are expressed as:

$$D = C_{\beta D}\, s\Delta, \text{ and} \quad (8)$$

$$R_F = C_{\beta R_F}\, \frac{S}{\Delta}\, \rho \min\left(1 - \frac{Y_F}{Y_{F0}}, 9\frac{Y_F}{Y_{F0}}\right). \quad (9)$$

Here, $C_{\beta D}$ and $C_{\beta RF}$ are model constants, s is the burning velocity, Δ is the control volume length in the direction of flame propagation and Y_{Fo} is the initial fuel mass fraction.

Turbulent burning velocity model

Correlations for the burning velocity are provided for different mixtures and flow regimes. The laminar burning velocity in both solvers, which is input to the burning velocity in all flow regimes, depends on the pressure as [6]:

$$s_L = s_{L0}\left(\frac{P}{P_0}\right)^{\gamma}, \tag{11}$$

where s_{L0} is the laminar burning velocity at atmospheric pressure, P_0, P is the pressure and γ is a fuel dependent parameter. To model the regime of cellular flame propagation, both solvers use the quasi-laminar burning velocity concept. In Flacs2, the quasi-laminar burning velocity is modelled as

$$s_{QL} = s_L\left(1 + C_{QL} r_F{}^a\right), \tag{12}$$

where s_{QL} is the quasi-laminar burning velocity, C_{QL} is a mixture-dependent model constant, r_F is the flame radius, a is a model constant. In Flacs3, the burning velocity in the quasi-laminar regime is given as

$$s_{QL} = s_L C^*_{QL}\left(\frac{r_F}{r_{F,cr}}\right)^{a^*}, \tag{13}$$

where $r_{F,cr}$ denotes the critical radius of the appearance of a cellular flame, and the model constants C^*_{QL} and a^* are both concentration- and mixture-dependent.

For the turbulent regime, a Markstein number-dependent burning velocity model is implemented in the Flacs3 solver. The turbulent burning velocity, S_T, is expressed in terms of the effective root-mean-square turbulence velocity, u_k', and the Karlovitz stretch factor K [8] as:

$$\frac{s_T}{u'_k} = \alpha\, K^{-\beta}, \qquad K = 0.25\left(\frac{u'}{s_L}\right)^2\left(\frac{u' l_C}{\upsilon}\right)^{-0.5} > 0.05, \tag{14}$$

where u' is the turbulence velocity, υ is the kinematic viscosity, l_C is the combustion length scale, and α and β are empirical parameters explicitly expressed in terms of the strain rate Markstein number. Thus, the variation in reactivity between various fuels and concentrations, including the response of the burning rate to varying flow properties, is accounted for when predicting the turbulent burning velocity. Flacs2 employs the turbulent burning velocity correlation proposed by Bray [9], which is on the same form as Equation (14) with fixed values for α and β. This correlation only accounts for differences in reactivity between various mixtures and concentrations through the laminar burning velocity.

According to Lipatnikov and Chomiak [10], s_T should increase with increasing pressure, despite the corresponding decrease in s_L. For the correlation described by Bradley *et al.* [8], this effect can be included through a pressure dependent Markstein number Ma and the kinematic viscosity υ. In Flacs3, the turbulent burning velocity varies with pressure according to the expression:

$$s_T^p = s_T\left(\frac{P}{P_0}\right)^b \tag{15}$$

where b is a model constant that has been fitted to match experimental measurements, and P_0 is a reference (initial) pressure. This correction is not applied in Flacs2.

Combustion length scale model

In Flacs2, the local turbulence length scale l_C used by the turbulent burning velocity correlation is proportional to the distance from the point of ignition to the flame front in many scenarios. For confined geometries, this growth is bounded by a parameter that is proportional to the distance between the enclosing walls. This simple model works reasonably well for single module configurations and many

confined scenarios but can result in unphysical results for flame propagation in unconfined and congested regions of high aspect ratio. However, test simulations with combustion length scales modelled via the turbulence length scale from the *k-ε* model did not give satisfactory results [11]. Therefore, in Flacs3, the combustion length scale is determined by a characteristic geometrical length scale of the sub-grid congestion, *GLS*, for grid cells where sub-grid obstructions are present. For uncongested grid cells, the current model system uses a simple combustion length scale model based on a wall distance formulation that decouples the resulting length scale from the employed turbulence model.

Flame wrinkling model

The flame wrinkling model accounts for the increase in burning velocity due to flame surface area generated by sub-grid obstructions. A frequently used approach for modelling flame folding due to sub-grid obstacles and flame instabilities entails the use of a transport equation [12] [13]. Flacs3 solves a transport equation for the relative increase in flame surface area generated by sub-grid obstacles, Ξ_s, based on modelling approaches presented by Weller *et al.* [14] and Puttock *et al.* [15].

$$\frac{\partial}{\partial t}(\rho\Xi_s) + \frac{\partial}{\partial x_i}(\rho u_i \Xi_s) = G_s\Xi_s - R_s(\Xi_s - 1), \tag{16}$$

where G_s and R_s are the generation and removal rates of Ξ_s, respectively. Flacs2 uses an equilibrium expression to represent this effect [6].

3.0 THE EXPERIMENTAL PROGRAMME

As part of the HySEA project, 20-foot ISO containers were filled with hydrogen using a circular pipe of 18 mm diameter (jet release) or a 200 mm square box (diffusive release). The flow rate was 56 m^3/h and the release was terminated after 450 s to achieve an average fuel concentration of 21%. The stratified mixtures were ignited at the back wall, about 2 m above the container floor, 30 s after the end of the release. The container roof had six openings. These were covered with either commercial pressure relief panels (6P) or with a plastic sheet (6O). The containers had a frame on the floor used to support obstacles (FO) or a pipe rack fixed to the frame (P2). Table 1 describes the configuration of the tests used for this validation study. Skjold [16] describes the experimental setup in detail.

Table 1. Experimental configurations.

Test	Configuration	Release	Duration (s)	Flow rate (m^3/h)	Venting
T41	FO	Diffusive	450	56	*
T44	FO	Diffusive	450	56	6P
T46	P2	**	**	**	6P
T57	FO	Jet	450	56	6P
T59	FO	Jet	450	56	6P
T60	P2	Jet	450	56	6P
T61	P2	Jet	450	56	6P

*Unignited test

** Reference test with homogeneous mixture

4.0 MODEL SETUP

Figure 1 illustrates the geometry model used for simulations for the container with the pipe rack together with the location of the monitor points. The monitor points E4, D4, C4, B4 and A4 correspond to sensors that measured the concentration continuously in the experiments. E4', D4', C4', B4' and A4' (not shown) were in a vertical line symmetric to E4-A4 and correspond to the concentration measured by a high specification process oxygen analyser. P1, P3, P5 and P7 (in yellow) are pressure sensors; P2, P4, P6 and P8 are respectively symmetrically arranged.

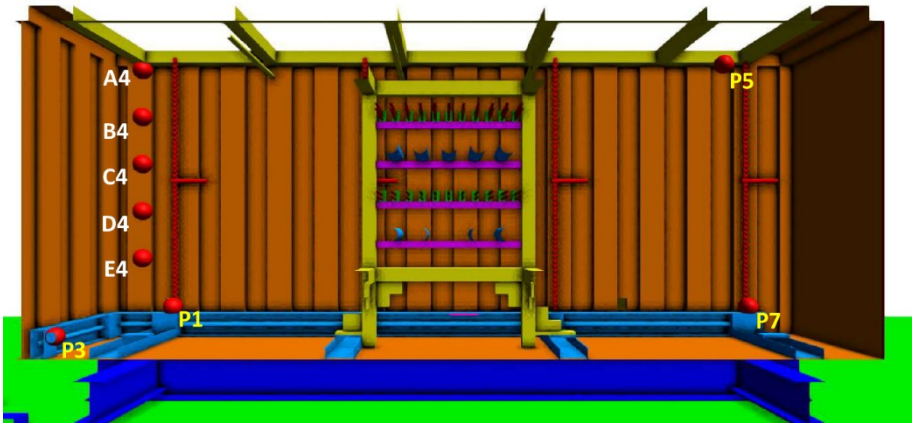

Figure 1. Geometry model section for the container with the pipe rack. The A4-E4 concentration measurement positions are represented in white; A4'-E4' are in a symmetrical vertical line. P1, P3, P5 and P7 (in yellow) are pressure sensors; P2, P4, P6 and P8 are respectively symmetrically arranged.

The grid resolution used inside the container was 10 cm. Guidelines for grid refinement around the leak were followed for dispersion simulations [3]. For explosion simulations, the simulation domain was extended, and the grid stretched towards the boundaries. The results obtained from dispersion simulations were used as input to the explosion simulations. The commercial panels were modelled as 6.8 kg/m^2 hinged panels with an opening pressure of 10 kPa.

5.0 RESULTS AND DISCUSSION

Figure 2 and Figure 3 show the comparison of the predicted hydrogen concentration with experimental data for sensors E4-A4 and E4'-A4'. The experimental results are labelled with a T followed by the test number (i.e. T57 corresponds to Test 57), cf. Table 1. The E4-A4 results for the first test are represented by dashed lines and the E4'-A4' by square dots. The repetition results are represented by dotted lines and diamonds. The hydrogen concentration results from both Flacs2 and Flacs3 were overlapping, since the models for dispersion in both solvers are identical. Here, the Flacs3 results are shown and represented by solid lines. The vertical lines indicate the end of the release (blue) and the time of ignition (red).

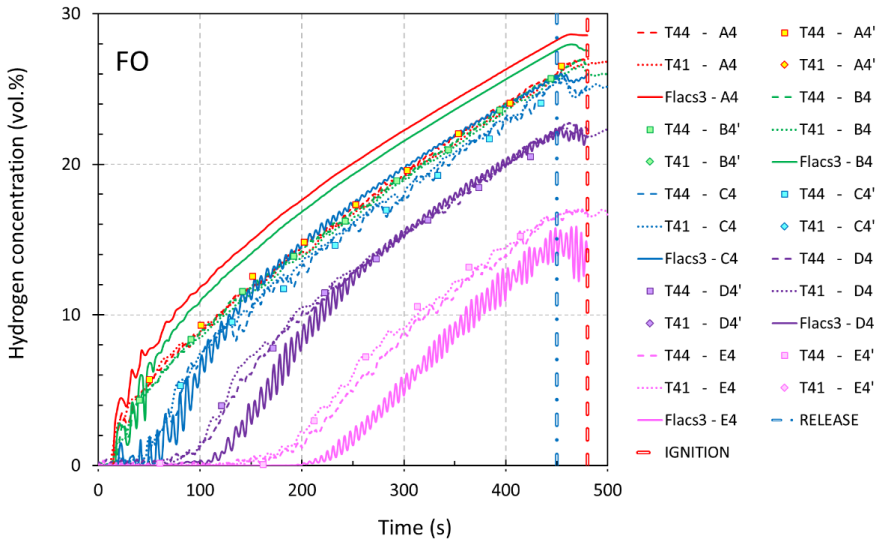

Figure 2. Hydrogen concentrations for the hydrogen release from the box in the empty container (FO).

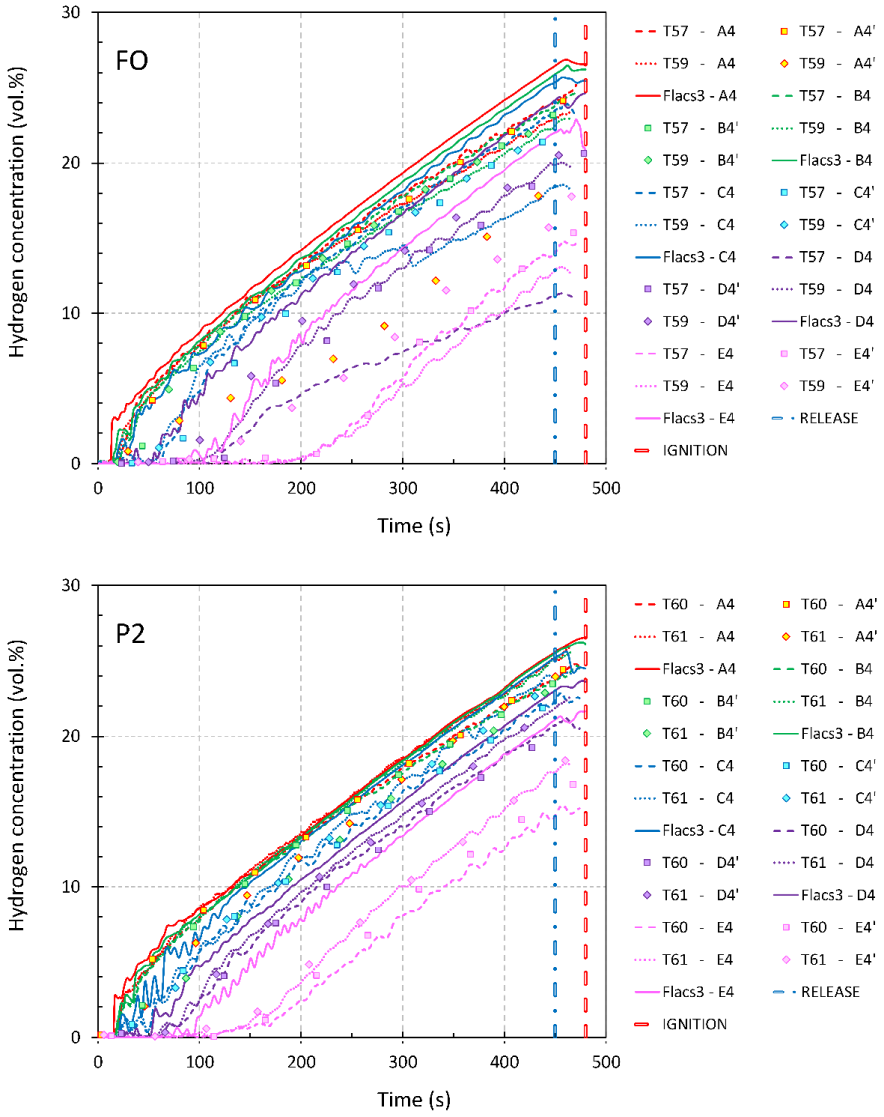

Figure 3. Hydrogen concentrations for hydrogen release from the pipe for both scenarios (FO and P2).

Flacs2 and Flacs3 reproduced the stratification observed in the experiments. A slightly lower concentration of hydrogen was reported for Test 57, Test 59 and Test 60 than for the corresponding unignited experiments with the same release [17]. For the monitor point E4, the concentration at the ignition time for Test 57 was about 2.3 vol.% lower than for the corresponding unignited test. Also, the concentration measured by the high specification process oxygen analyser differed from the concentration measured by the continuous measurement at monitor points D4 and E4, in particular for Test 59. Loss of hydrogen in the experiments may explain the over-prediction of hydrogen concentrations observed in the simulations. FLACS reproduced the clouds generated by the release from the box better than that clouds generated by a jet release. The diffuse leak in FLACS applies the surrounding flow velocity to the leaking gas. However, for the jet leak, the temperature of the outflow is used to obtain the velocity of the outflow. This assumption introduces additional uncertainty to the modelling.

Table 2 summarises the results for the explosion simulations. The maximum overpressures from the first experiment and the repetition, if any, are shown together with the predicted maximum overpressure by Flacs2 and Flacs3. The description of the case indicates the obstacles in the container (P2 or FO), the venting (6P or 6O), the leak source (jet or leak), the average hydrogen concentration and whether the mixture in the container was homogeneous or inhomogeneous. For Test 57 and Test 59, the panel opening pressure (estimated from video recordings), was found to be about 8 kPa (rather than 10 kPa).

Additional simulations with panel opening pressures of 8 kPa resulted in a reduction in predicted peak overpressure of about a 10 kPa.

Table 2. Maximum peak overpressure summary.

Case	Maximum peak overpressure (kPa)			
	Flacs2	Flacs3	Experiment	Repetition
P2, 6P, Jet, 21 % Inhomogeneous	1153	112	*(T60)* 37	*(T61)* 68
FO, 6P, Jet, 21 % Inhomogeneous	655	80 / 70[a]	*(T57)* 34	*(T59)* 34
FO, 6P, 21 % Homogeneous	60	25	*(T46)* 19	*(T47)* 20
FO, 6P, Diffusive, 21 % Inhomogeneous	437	79	*(T44)* 41	-

[a] **Simulation with panel opening pressure of 8 kPa**

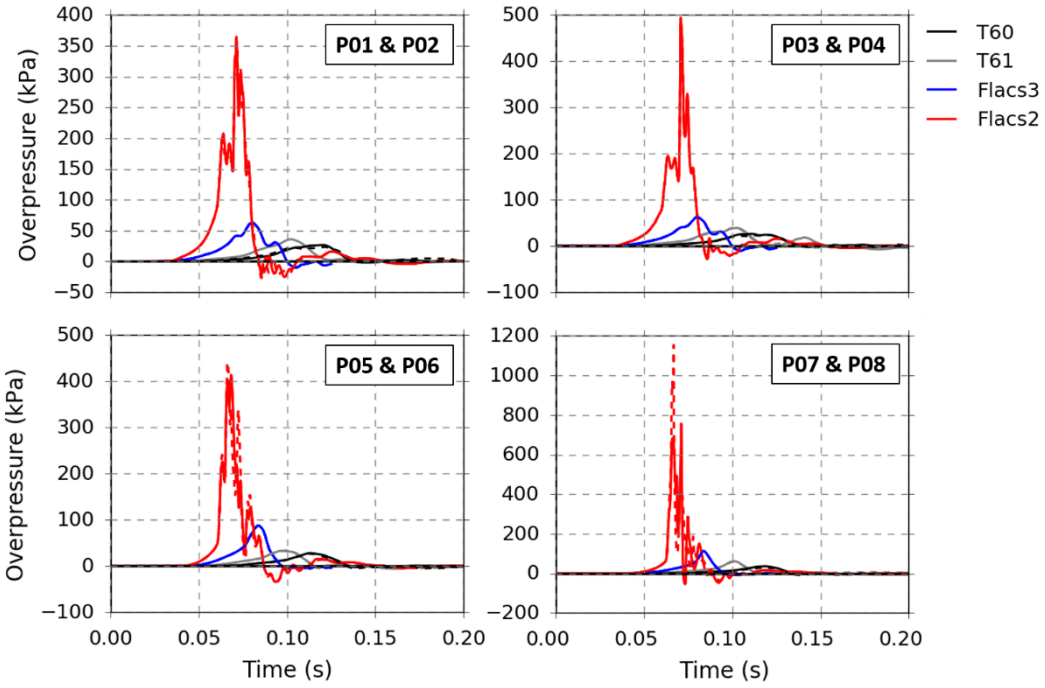

Figure 4. Predicted pressure-time histories and experimental results for tests with a jet release of hydrogen, commercial vent panels and a pipe rack inserted in the container.

Figure 4 and Figure 5 show the overpressure-time curves for the tests with a jet release. The experimental results are represented by black and grey lines. The Flacs2 results are represented by red lines and Flacs3 results by blue lines. The monitor points P01, P03, P05 and P07 are represented by solid lines and their symmetric counterparts (P02, P04, P06 and P08, respectively) by dashed lines. Figure 4 and Figure 5 show the overpressure-time histories for the tests with the 450 s release from the pipe, using six commercial vent panels. Test 60, 61, 57 and 59 were part of the 2nd Blind Prediction of the HySEA project [17] and had a nominal average hydrogen concentration of 21%. Test 60 and Test 61 were performed with a pipe rack inside the container. Figure 6 shows the overpressure recorded for Test 44, with ignition after 450 s of a 56 m^3/h diffusive hydrogen release, a pipe rack in the container and the vent openings covered by plastic sheets.

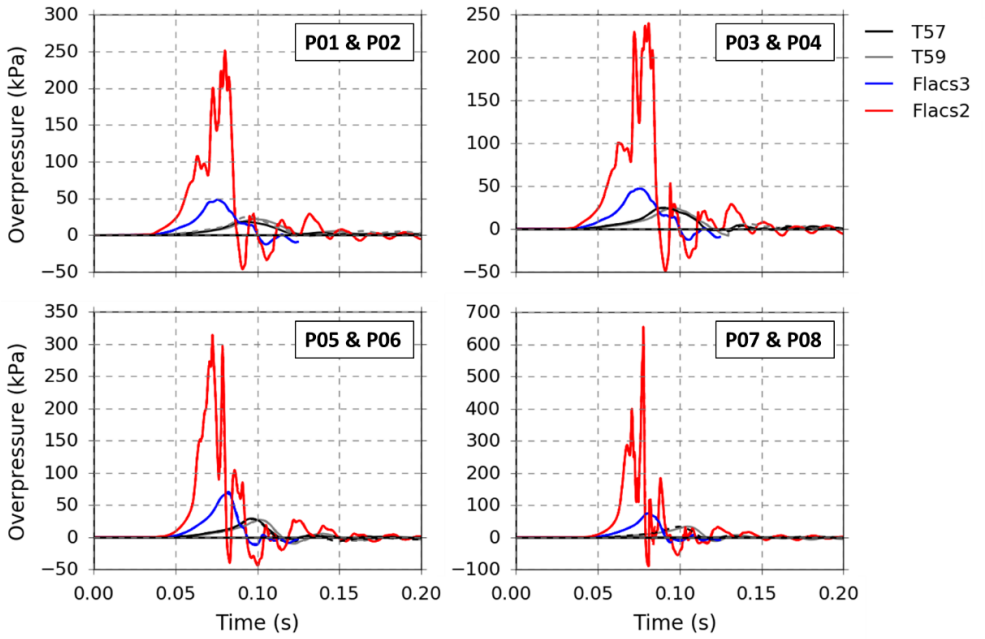

Figure 5. Predicted pressure-time histories and experimental results for tests with a jet release of hydrogen, commercial vent panels and only the frame inserted in the container.

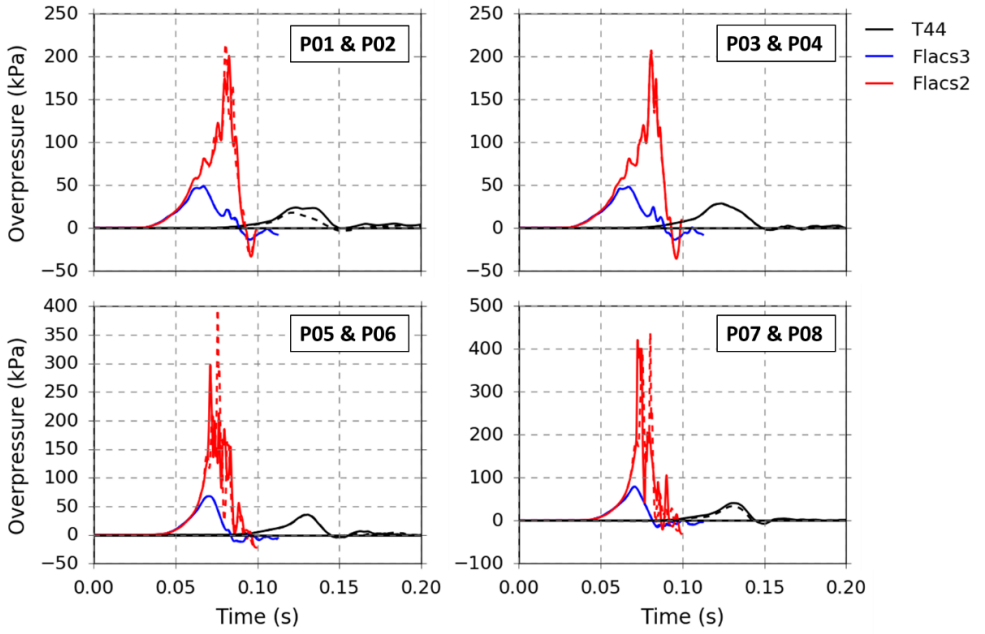

Figure 6. Predicted pressure-time histories and experimental results for tests with a diffusive release of hydrogen, commercial vent panels and only the frame inserted in the container.

As presented in Table 2, Figure 4 and Figure 5, the significant over-prediction of explosion overpressure by FLACS *v10.9* and FLACS *v10.8* (using the Flacs2 solver and presented in the 2nd Blind Prediction of the HySEA project [17]) was considerably reduced in simulations with FLACS *v11 beta* (using the Flacs3 solver).

Figure 7 shows the flame speed for simulations representing the scenario in tests 60 and 61. The flame speed was calculated using the distance from the ignition point to the location of the isotherm corresponding to 1200 K. Figure 7 shows that from the time of ignition, the flame speed predicted by Flacs2 is higher than that predicted by Flacs3. In the early phase of flame propagation, before the flame front reaches the pipe rack, the quasi-laminar burning velocity governs the flame propagation for both

FLACS versions. For tests 60 and 61, in the region before the pipe rack, the quasi-laminar burning velocity predicted by Flacs2 is about 2 m/s higher than that predicted by Flacs3. Once the flame enters the congestion region, the flame acceleration is significantly higher for Flacs2 than for Flacs3. Here, both the flame folding due to sub-grid obstructions and the turbulent burning velocity models in the two solvers are different. The turbulent burning velocity model in Flacs2 predicts a burning velocity at the time of peak pressure that is 17% higher than the model in Flacs3.

For hydrogen-air mixtures, Flacs2 applies a Lewis number dependent correction directly to the laminar burning velocity [18], resulting in an enhancement in the laminar burning velocity for lean mixtures and a reduction in the laminar burning velocity for rich mixtures [19]. This correction thus accounts for Lewis (or Markstein) number dependent effects for hydrogen-air flames in all flow regimes, and most likely contributes to the over-prediction of the reactivity of lean hydrogen-air mixtures with a fuel concentration ranging from around 18-24 vol% [19][20]. Meanwhile Flacs3 accounts for Lewis/Markstein-number dependent effects for each regime of flame propagation separately. Overall, Flacs2 predicts higher values for the laminar and quasi-laminar burning velocities than Flacs3 for hydrogen-air mixtures in the concentration range involved in these tests. The model for the combustion length scale in Flacs2 also yields higher values for the turbulence combustion length scale l_C, which is used as input to the turbulent burning velocity correlation. The maximum overpressure observed in the experiments occurred at about 25 ms after the panels opened, while Flacs3 predicts that the maximum overpressure occurs around 30 ms after the panels open. The vent panels in the Flacs3 simulations open before the flame front reaches the pipe rack. At the time of maximum pressure in the container, the simulated flame front has propagated through the pipe rack.

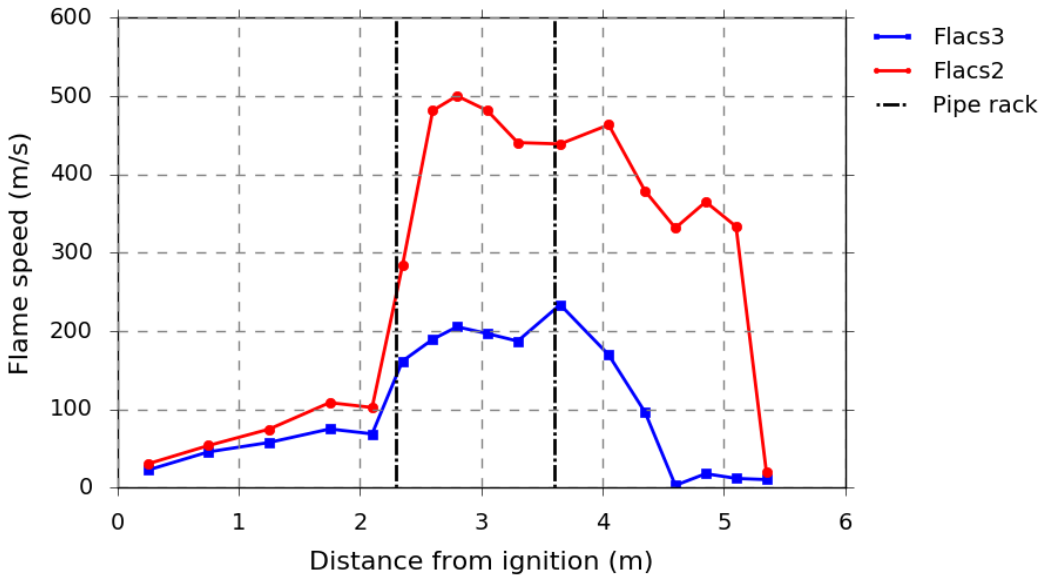

Figure 7. Simulated flame speed for Tests 60 and 61.

The maximum peak overpressures for homogeneous mixtures (Test 46 and Test 47 in Table 2) were considerably lower than for the inhomogeneous mixture tests with the same amount of fuel (Tests 60 and Test 61), for both experiments and simulations. In particular, the over-prediction of pressures by Flacs2 was less pronounced for homogeneous than for inhomogeneous mixtures. Lakshmipathy *et al.* [20] presented maximum overpressures from Flacs2 simulations that were highly over-predicted for homogeneous mixtures with 24 vol.% hydrogen in air. The hydrogen concentration near ignition for stratified mixtures in this study exceeded 24 vol.%. This partly explains the significant over-prediction of pressures in simulations using Flacs2 in tests with inhomogeneous mixtures, with an average concentration of 21 vol.%.

The stratified hydrogen mixture used as input to the explosion simulations (Figure 2 and Figure 3) had an overall higher concentration than that observed in the experiments. For lean mixtures, higher concentrations generally lead to higher peak pressures. To investigate this sensitivity, two user defined stratified clouds were used as input to the scenario in Test 60 with an overall difference of 2 vol.% hydrogen in air. The peak overpressure was reduced by 2 kPa when the overall hydrogen concentration was reduced. This suggest that some of the over-prediction of overpressure is due to over-predicted hydrogen concentrations.

6.0 CONCLUSION

A validation study for the new solver Flacs3 (used in FLACS *v11 beta*) was performed and compared to results from the Flacs2 solver (used in FLACS *v10.9*). Both model versions predict the release and dispersion of hydrogen inside 20-foot shipping containers with reasonable accuracy. Flacs2 significantly over-predicts the explosion pressure for ignited clouds generated by realistic hydrogen releases. The new combustion models in the Flacs3 solver improves the predictions. Overall, the peak overpressures predicted by Flacs3 were within a factor of 2 [21] of the experimental results. For the same average concentration of hydrogen in the container, the peak overpressure was higher for scenarios with stratified than for homogeneous mixtures. The hydrogen losses from the container prior to ignition in the experiments were unknown, and the overall fuel concentration was slightly over-predicted by the models. This may have contributed to the subsequent over-prediction of explosion overpressure.

Some parameters in the sub-grid models are found using a parameter optimization routine [22] that includes a wide range of explosion experimental campaigns with different fuels. Hydrogen has not been included in the parameter optimization for Flacs2 or Flacs3. Further work will focus on extending the automated hydrogen validation database to be used in parameter optimization using medium- and large-scale hydrogen experiments.

ACKNOWLEDGEMENTS

The HySEA project received funding from the Fuel Cells and Hydrogen 2 Joint Undertaking (FCH 2 JU) under grant agreement No 671461. This Joint Undertaking received support from the European Union's Horizon 2020 research and innovation programme and the United Kingdom, Italy, Belgium and Norway.

REFERENCES

1. EN 14994:2007, Gas Explosion Venting Protective Systems, 2007 edition, BSI, UK, 2007.
2. NFPA 68, Standard on explosion protection by deflagration venting, 2013 edition, National Fire Protection Association, NFPA, Massachusetts, 2013.
3. Gexcon. FLACS User's Manual v10.9, Gexcon, Bergen, 2019.
4. Hjertager, B., Handbook of heat and mass transfer (Cheremisinoff, N.P. Eds.), Gulf Publishing Company, Houston, 1986, pp. 1303.
5. Patankar S.V. and Spalding, D.B., Heat exchangers: Design and theory sourcebook (Afgan, N. and Schlünder, E.U. Eds.), McGraw-Hill, New York, 1974, pp. 155.
6. Arntzen, B, Modelling of turbulence and combustion for simulation of gas explosions in complex geometries. PhD thesis, Department of Energy and Process Engineering, Norwegian University of Science and Technology, 1998, Norway.
7. Launder, B.E., and Spalding, D.B., The numerical computation of turbulent flows, *Computer Methods in Applied Mechanics and Engineering*, **3**, No 2, 1974, pp. 269–289
8. Bradley, D., Lawes, M., Liu, K. and Mansour, M., Measurements and correlations of turbulent burning velocities over wide ranges of fuels and elevated pressures, *Proceedings of the Combustion Institute*, **34**, No 1, 2013, pp. 1519-1526.
9. Bray, K.N.C., Studies of the turbulent burning velocity, *Proceedings: Mathematical and Physical Sciences*, **431**, No 1882, 1990, pp. 315-335.

10. Lipatnikov, A. and Chomiak, J., Turbulent flame speed and thickness: phenomenology, evaluation, and application in multi-dimensional simulations, *Progress in Energy and Combustion Science*, **28**, No 1, 2002, pp.1-73.
11. Skjold, T., Hisken, H., Atanga, G., Narasimhamurthy, V.D., Lakshmipathy, S., Storvik, I.E., Pesch, L., and Braatz, A.-L., Modelling escalating accident scenarios and the use of risk-reducing technology for explosion safety (MEASURE), GEXCON Report No. Gexcon-17-F46241-C1.
12. Bauwens, C. and Dorofeev, S., Experimental and numerical study on the effect of mixture composition on vented explosions, Proceedings of the Sixth International Seminar on Fire & Explosion Hazards, 11-16 April, 2011.
13. Keenan, J., Makarov, D., and Molkov, V., Rayleigh taylor instability: Modelling and effect on coherent deflagrations, *International Journal of Hydrogen Energy*, **39**, No 35, 2014, pp. 20467-20473.
14. Weller, H.G., Tabor, G., Gosman, A.D., and Fureby, C., Application of a flame-wrinkling LES combustion model to a turbulent mixing layer, *Symposium (International) on Combustion*, **27**, No 1, 1998, pp. 899-907
15. Puttock, J., Chakraborty, D., and Farmayan, W., Gas explosion modelling using PDRFoam, Tenth International Symposium on Hazards, Prevention, and Mitigation of Industrial Explosions, 10-14 June, 2014, Paper. 122.
16. Skjold, T., Vented hydrogen deflagrations in 20-foot ISO containers, Proceedings Twelfth International Symposium on Hazards, Prevention and Mitigation of Industrial Explosions, 12-17 August, 2018, pp. 823-846.
17. Skjold, T., Hisken, H., Bernard, L., Mauri, L., Atanga, G., Lakshmipathy, S., Lucas, M., Carcassi, M., Schiavetti, M., Rao, V.C.M., Sinha, A., Tolias, I.C., Giannissi, S.G., Venetsanos, A.G., Stewart, J.R., Hansen, O.R., Kumar, C. and Krumenacker, L.L., Blind-prediction: estimating the consequences of vented hydrogen deflagrations for inhomogeneous mixtures in 20-foot ISO containers, Journal of Loss Prevention in the Process Industries, **61**, 2019, pp. 220-236.
18. Middha, P., Development, use, and validation of the CFD tool FLACS for hydrogen safety studies, PhD thesis, Department of Physics and Technology, University of Bergen, Norway, 2010.
19. Hisken, H., Investigation of instability and turbulence effects on gas explosions: experiments and modelling, PhD thesis, University of Bergen, 2018.
20. Lakshmipathy, S., Skjold, T., Hisken, H. and Atanga, G., Consequence models for vented hydrogen deflagrations: CFD vs. engineering models. International Journal of Hydrogen Energy, **44**, No 17, 2019, p.p. 8699-8710
21. Hisken, H., Atanga, G., Skjold, T., Lakshmipathy, S., and Middha, P., Validating, documenting and qualifying models used for consequence assessment of hydrogen explosion scenarios. Eleventh International Symposium on Hazard, Prevention and Mitigation of Industrial Explosions, 24-29 July, 2016.
22. Both, A.-L., Gordon, A. and Hisken, H., CFD modelling of gas explosions: optimising sub-grid model parameters, *Journal of Loss Prevention in the Process Industries*, **60**, 2019, pp. 159-173.